Articles

Roles of Dimerization Domain Residues in Binding and Catalysis by Aminoacylase-1†

Holger A. Lindner,* Alain Alary, Lorena I. Boju, Traian Sulea, and Robert Ménard

Biotechnology Research Institute, National Research Council of Canada, Montréal, Québec, Canada H4P 2R2

Received June 20, 2005; Revised Manuscript Received September 30, 2005

ABSTRACT: The aminoacylase-1/metallopeptidase 20 (Acy1/M20) family is the largest metallopeptidase family. Several crystal structures feature a metal-binding and a dimerization-mediating domain, both arranged in an extended open conformation. We have recently shown [Lindner et al. (2003) *J. Biol. Chem. 278*, 44496−44504] that in human Acy1 the invariant residues Glu147 and His206 from the metal-binding and the dimerization domain, respectively, are recruited to the active site from opposite dimer subunits. We hypothesized that, to facilitate this, formation of the binary complex is associated with domain closure, which would also position additional residues in the functional active site of Acy1. These would include two partially conserved dimerization domain residues: an asparagine (Asn263) and an arginine (Arg276) from the same subunit as His206 and Glu147, respectively. In this paper, we investigate the significance of the three dimerization domain residues of human Acy1 His206, Asn263, and Arg276 and, additionally, the nearby Asp274 for catalysis using site-directed mutagenesis. Enzyme complementation assays confirm the putative subunit allocations of these residues, and steady-state kinetics support roles for all of them in catalysis but only involve the Arg276 in substrate-binding. The results are consistent with a model of the closed conformation for the structure of the related enzyme carboxypeptidase G2. This study demonstrates experimentally for the first time for a member of the Acy1/M20 family that several residues outside of the metal-binding domain are involved in binding and catalysis.

The aminoacylase-1/metallopeptidase 20 (Acy1/M20)[1] family from the metallopeptidase H (MH) clan represents the largest group of metallopeptidases based on sequence similarity. The MEROPS database of peptidases (http://merops.sanger.ac.uk) (*1*) records over 1000 sequences for this family from all kingdoms of life. Mammalian Acy1 (EC 3.5.1.14), the first enzyme from the family to be described (*2*), is a ubiquitous enzyme which functions in the salvage of Nα-acetylated amino acids from protein degradation (*3*). Recently, porcine Acy1 was shown to also deacylate certain quorum-sensing *N*-acylhomoserine lactones (*4*), and the rat enzyme was implicated in the degradation of chemotactic peptides of commensal bacteria (*5*). In biocatalysis, high stereoselectivities allow the use of porcine kidney Acy1 (*6*, *7*) and a related L-aminoacylase from *Thermococcus litoralis* (*8*) in the preparation of enantiomerically pure amino acids.

The Acy1/M20 family further includes several members with different metabolic functions and therapeutic significance. The bacterial enzymes PepV (EC 3.4.13.3) and PepT (EC 3.4.11.14), for example, function in amino acid utilization (*9*, *10*), whereas bacterial allantoate amidohydrolase (EC 3.5.3.9) (*11*) and yeast βAS (EC 3.5.1.6) (*12*) are enzymes of the purine and pyrimidine catabolic pathway, respectively. Bacterial DapE (EC 3.5.1.18) and ArgE (EC 3.5.1.16) are involved in the succinylase pathway and the arginine biosynthetic pathway (*13*, *14*), respectively, and are both considered as potential targets of antimicrobial agents (*15*). Last but not least, CPG2 from *Pseudomonas* sp. strain RS-16 (EC 3.4.17.11) is currently under development as a rescue agent (Voraxaze) in cases of methotrexate overdoses.

Several available crystal structures for microbial Acy1/M20 family enzymes, including CPG2, show a dizinc-binding domain, which is characteristic for the MH clan of cocatalytic zinc peptidases, and a typical smaller domain, which is inserted in the middle of the metal-binding domain and mediates homodimerization (*12*, *16*, *17*).[2] In each of these structures, the two domains display an extended open conformation. Acy1 shows the same overall two-domain organization, and also forms a homodimer (*18*−*20*), but so far, only the structure of the metal-binding domain could be solved for the human enzyme (T347G mutant) (*19*).

PepV from *Lactobacillus delbrueckii* also features two enzyme domains but exists as a monomer (*21*). PepV is also

† This is NRCC publication no. 47483.

* Corresponding author. Phone: 514-496-1887. Fax: 514-496-5143. E-mail: Holger.Lindner@cnrc-nrc.gc.ca.

[1] Abbreviations: Acy1, aminoacylase-1; ArgE, *N*-acetyl-L-ornithine deacetylase; βAS, β-alanine synthase; CPG2, carboxypeptidase G2; DapE, *N*-succinyl-L, L-diaminopimelate desuccinylase; PepT, amino tripeptidase T; PepV, peptidase V.

[2] Structural GenomiX, Inc. (San Diego, CA), PDB code 1VGY, unpublished results.

10.1021/bi051180y CCC: $30.25
Published on Web 11/08/2005

Table 1: Forward Versions of Mutagenic Primers for Human Acy1, and Sequence Conservation of the Mutated Residues in the Acy1/M20 Family

Acy1 mutant	oligonucleotide sequence[a]	degree of residue conservation[b]
H206A	5′-GGGAGGCCAGGCGCTGCCTCACGCTTC-3′	100%
H206K	5′-CTGGGAGGCCAGGCAAGGCCTCACGCTTC-3′	
N263A	5′-GGGTGGCGTGGCCTATGCCGTGATACCTGCCACC-3′	84%
N263S	5′-GGCGTGGCCTATAGCGTGATACCTGCC-3′	
N263D	5′-GGGTGGCGTGGCCTATGACGTGATACCTGCCACC-3′	
R276A	5′-GCCAGCTTTGACTTCGCTGTGGCACCGGATG-3′	52%
R276N	5′-GCGCCAGCTTTGAGTTCAATGTGGCACCGGATGTGG-3′	
R276Q	5′-GCGCCAGCTTTGACTTCCAGGTGGCACCGGATGTGG-3′	
D274A	5′-GCGCCAGCTTTGCCTTCCGTGTGGC-3′	19%[c]

[a] Altered nucleotides, that introduced the desired mutations, are underlined. [b] The degree of conservation for the mutated residue in human Acy1 among 281 members of the Acy1/M20 family, as aligned in the MEROPS database (http://merops.sanger.ac.uk) (*1*), is indicated. [c] Asparagine, not aspartic acid, is the prevailing amino acid at position 274, with a conservation level of 34%.

the only member of the Acy1/M20 family for which the structure of a complex with an inhibitor has been solved (*21*). A dipeptide transition-state mimetic (AspΨ[PO_2CH_2]AlaOH) was cocrystallized and is bound in a cavity created by the two enzyme domains in a closed conformation. Enzyme−ligand interactions in the complex include the dinuclear zinc center and a glutamate residue in its immediate vicinity (*21*), which is conserved throughout the MH clan and is believed to function as a general acid−base catalyst (*19*, *22*). Notably, the structure also implicates residues from the small domain in substrate binding and catalysis, including an invariant histidine, that appears to stabilize the tetrahedral reaction intermediate by oxyanion-binding (*21*). We have previously recognized that the small domain of PepV contains two subdomains, which in fact mimic the arrangement of two dimerization domains within a dimer (*19*). In the available dimer structures, however, the mentioned histidine does not approach the corresponding zinc center in the opposite subunit by more than 7 Å due to their open domain conformations (*12*, *16*, *17*),[2] and its potential significance for catalysis is, therefore, not obvious. Nevertheless, our recent mutational analysis of human Acy1 support a role for this residue in catalysis, which we showed to occur at the dimer interface (*19*). To explain active site formation in dimeric enzymes of the Acy1/M20 family, we hypothesized that domain closure, possibly induced by substrate binding, facilitates the appropriate structural alignment of otherwise distant residues in the active site. We predicted (*19*) that these would include, besides the above-mentioned glutamate and histidine, two partially conserved dimerization domain residues: an arginine and an asparagine from the same subunit as the glutamate and the histidine, respectively.

In this paper, we probed the proposed conformational transition for the structure of the CPG2 dimer from a structural viewpoint by molecular modeling. We experimentally tested the significance of the putative active site residues His206, Asn263, and Arg276 and, additionally, Asp274 in the dimerization domain of human Acy1 using site-directed mutagenesis, enzyme complementation, and steady-state kinetics. Our results confirm that dimerization is important for active site formation and show that this occurs through the contributions of residues from the dimerization domains of both enzyme subunits and one metal-binding domain. Kinetic parameters suggest roles for all the mutated residues in catalysis but only involve the arginine in substrate-binding.

MATERIALS AND METHODS

Model Building and Refinement. Detailed procedures for the building of the substrate-bound model of CPG2 are given in the Supporting Information of this report. Structural manipulations and preparation were performed with the SYBYL 6.9 molecular modeling software (Tripos, Inc., St. Louis, MO). In brief, the structures of one metal-binding domain and two dimerized insertion domains of CPG2 were independently superimposed on the corresponding parts of the PepV structure by least-squares fitting of selected atom pairs. The metal-binding domain and the insertion domain of one CPG2 subunit were then rejoined at breakage points within the presumably flexible linker regions. The substrate 4-(diethylamino)benzoylglutamate was initially docked into the active site of the resulting preliminary closed-conformation model of CPG2 as a tetrahedral intermediate, following the binding mode of the transition-state inhibitor AspΨ-[PO2CH2]AlaOH in the active site of the PepV structure. The model of the complex was then refined using a stepwise protocol of energy minimization with the AMBER all-atom molecular mechanics force field (*23*).

Preparation of Acy1 Mutants. Site-directed mutagenesis of human Acy1 was performed on the baculovirus transfer vector pVL1393-hAcI (*24*) using the QuikChange XL Site-Directed Mutagenesis Kit (Stratagene, La Jolla, CA). Forward versions of the mutagenic primers are listed in Table 1. The sequences of the mutant Acy1 genes in the resulting transfer vectors were confirmed by DNA sequencing. Wild-type Acy1 and its variants were expressed in a baculovirus expression vector system and purified as described (*24*). In brief, 300 mL cultures of infected Sf21 cells were harvested 72 h after infection. Cells were disrupted by sonication, and enzyme was purified by column chromatography on phenyl−Sepharose CL-4B and Q-Sepharose fast flow (Amersham Biosciences, Piscataway, NJ). Enzyme preparations were stored at −80 °C and used for activity measurements within 8 weeks, when there were no signs of degradation as judged by SDS−PAGE.

Protein Characterization. Protein concentrations were determined using the Bio-Rad (Hercules, CA) protein assay based on the original Bradford assay (*25*) with bovine serum albumin as the standard. Proteins were separated in 13% Laemmli-type SDS gels, using BenchMark Protein Ladder (Invitrogen, Burlington, ON) as a marker for apparent molecular weights and Coomassie R350 for staining. Ap-

parent molecular weights after long-term storage were also estimated by analytical gel filtration at room temperature. First, protein samples were transferred into 50 mM potassium phosphate, pH 7.0, and 150 mM sodium chloride using a NAP-5 column (Amersham Biosciences). Aliquots of 200 μL, containing 20−30 μg of protein, were applied to a Superdex 200 HR column (1 cm × 30 cm) (Amersham Biosciences), equilibrated with the same buffer, at a flow rate of 0.7−0.8 mL/min. For calibration, dextran blue, chymotrypsinogen A (25 kDa), ovalbumin (43 kDa), albumin (67 kDa), and aldolase (158 kDa) were selected from molecular weight calibration kits (Amersham Biosciences).

Acy1 Activity Assay. Acy1 amino acid deacylating activity was determined at pH 7.4 by a discontinuous colorimetric assay as described previously (*24*). Steady-state kinetics were evaluated by nonlinear regression analysis with the Michaelis−Menten equation ($v = V_{max}[S]/(K_M + [S])$), using the SigmaPlot software (SPSS Science, Chicago, IL). The catalytic constant, k_{cat}, was calculated using the equation $V_{max} = k_{cat}[E]$, where [E] = total enzyme concentration. In situations, where the rates versus substrate concentration plots showed no curvature, that is, measurements were obviously performed far below K_M, the k_{cat}/K_M values were obtained by dividing the slopes by the enzyme concentrations. The enzyme complementation assay was carried out as described previously (*19*). Briefly, enzyme mutants were mixed at equimolar ratios (120 μg/mL). After an equilibration period of 16 h, samples were assayed for *N*α-acetyl-L-methionine (10 mM)-hydrolyzing activity.

RESULTS AND DISCUSSION

Production of Acy1 Mutants. To elucidate the putative contributions of dimerization domain residues to the active site in human Acy1, we first examined the available three-dimensional structures of related enzymes (*12*, *16*, *17*, *21*).[2] The structure of the monomeric Acy1/M20 family enzyme PepV in complex with the dipeptide transition-state mimetic AspΨ[PO_2CH_2]AlaOH identified, besides residues in the metal-binding domain, three residues in the small enzyme domain, His269, Arg350, and Asn217, that interact with the ligand (*21*). As already mentioned, in dimeric Acy1/M20 family members, we previously mapped equivalent residues (His206, Arg276, and Asn263, respectively, in human Acy1) to the dimerization domain and hypothesized that they become inserted into the active site, defined by the dinuclear zinc center, only upon domain closure (*19*). Here, we assessed the structural feasibility of such a transition from the open to a closed conformation for a dimeric Acy1/M20 family enzyme by molecular modeling based on the PepV−inhibitor complex (*21*). In the absence of a structure for full-length Acy1, we chose the structure of the CPG2 dimer (*16*) for this. A closed conformation, similar to that seen in the monomeric PepV (*21*), could be modeled for the dimeric CPG2 in complex with a transition-state substrate (4-(diethylamino)bezoylglutamate) bound in an interdomain cavity, created upon domain closure and containing the zinc center (Figure 1A). In the model, the dimerization domain residues Arg288, from the same dimer subunit as the zinc center, and His229 and Asn275, from the opposite subunit, become positioned in the vicinity of the substrate (Figure 1B), supporting potential roles as active site residues. A more detailed interpretation of the modeled transition-state adduct for CPG2 is provided in the Appendix.

We used site-directed mutagenesis to test the roles of the equivalent dimerization domain residues, which show different degrees of conservation in the Acy1/M20 family, in human Acy1 (Table 1). In addition to our previously described asparagine mutant of His206 (*19*), we constructed alanine and lysine variants, introducing more pronounced structural changes at this position. Arg276 was mutated to alanine, asparagine, and glutamine and Asn263 to alanine, serine, and aspartate. The properties of an additional N263Q mutant (not described further) were the same as for the N263S mutant. Furthermore, we replaced Asp274 by an alanine because of a possible orientation effect of this residue on Arg276 through the formation of a salt bridge, as seen in the crystal structures of CPG2 (*16*) and βAS (*12*).

The mutants H206A, H206K, N263S, N263D, R276A, R276N, R276Q, and D274A showed the same expression and purification behavior as the wild-type enzyme and appeared homogeneous as assessed by SDS−PAGE (not shown). For the N263A mutant, however, a major band at an apparent molecular weight of 30 kDa, instead of the expected 45 kDa for full-length Acy1 (*24*), was visible already in the whole cell extract of the expression culture. This indicated sensitivity of this protein to proteolysis precluding further analysis. For the remaining, purified mutant proteins, but not the wild-type, SDS−PAGE analysis revealed additional lower molecular weight bands only after storage at −80 °C for 6−8 months (Figure 2). The most obvious of these were apparent at about 35 or 26 kDa. Given the marked resistance of the ∼25 kDa zinc-binding domain of Acy1 against proteolysis (*19*, *20*, *26*), these degradation products likely comprise this domain. Determination of apparent molecular weights by analytical gel filtration, nevertheless, confirmed the presence of the 90 kDa enzyme dimer for all these mutants after the storage period, accounting for at least 85% of the total eluted protein. Collectively, all of our analyzed mutants were stable in the time period required to perform the functional assays and showed marginally increased susceptibility to degradation only after prolonged storage.

Steady-State Kinetics of Acy1 Mutants. Kinetic measurements were performed using *N*α-acetyl-L-methionine as the substrate. Table 2 summarizes the kinetic parameters, including those of the previously characterized H206N mutant (*19*). An over 11 000-fold loss in catalytic efficiency (k_{cat}/K_M) for this mutant had already implicated His206 in catalysis. Although less pronounced, 560- and 350-fold losses in catalytic efficiency due to reduced k_{cat} values for the H206A and H206K mutant, respectively, also support a role for His206 in catalysis. Similarly, a 150-fold loss in k_{cat}/K_M for the N263S mutant suggests a role for this residue during catalysis. No activity at all could, however, be detected for the N263D mutant.

Mutation of Arg276 to alanine, asparagine, or glutamine led to the greatest observed reductions in k_{cat}/K_M ranging from 4 to 5 orders of magnitude (Table 2). The substrate-dependent rates of hydrolysis for the R276N and R276Q mutants increased in an apparently linear manner up to 20 mM of substrate, reflecting highly increased Michaelis constants (K_M) and, therefore, marked losses of affinity for the substrate. Kinetics for the R276A mutant still showed

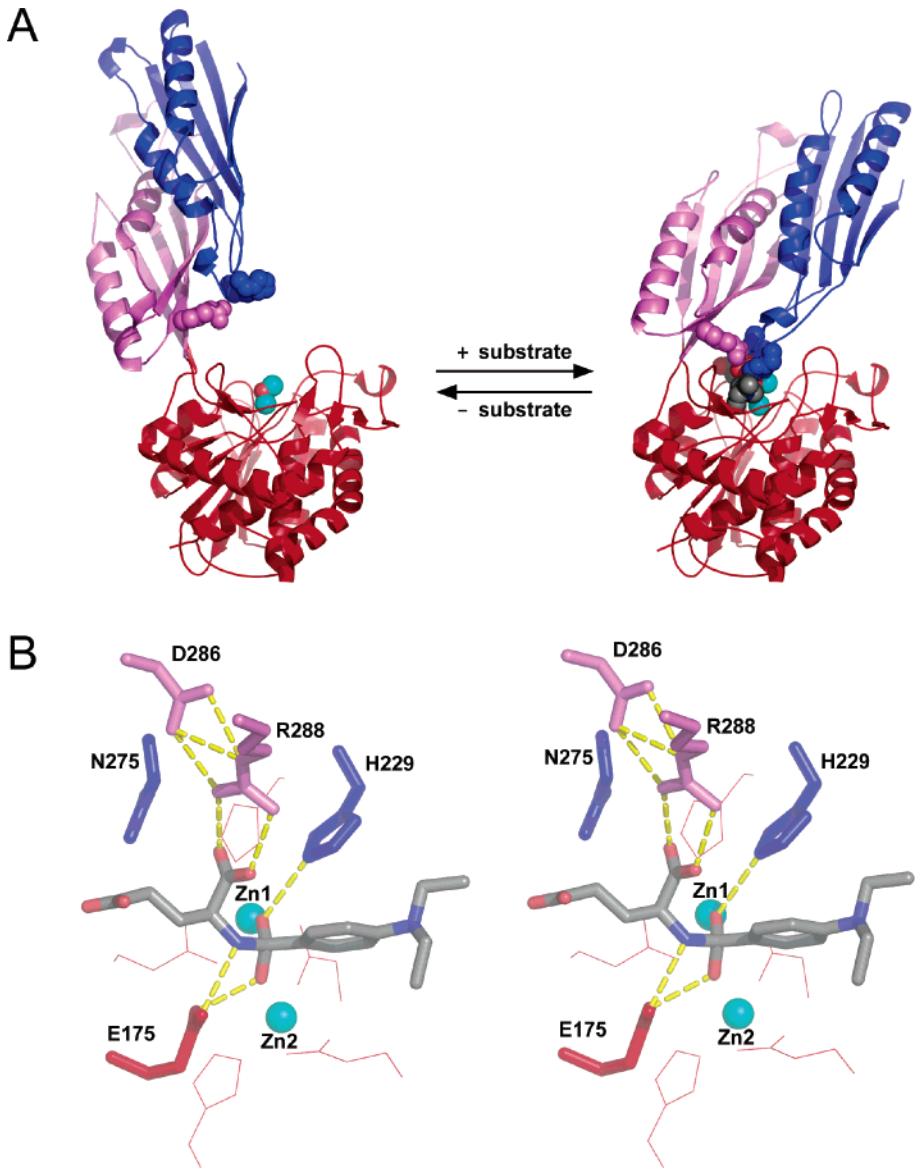

FIGURE 1: Structural model for the active conformation of M20-family dimeric enzymes. (A) Conformational switch during catalysis in CPG2. In the crystal structure of CPG2 (PDB ID 1CG2, on the left), the two enzyme domains assume an open conformation relative to each other. Upon addition of the substrate, the dimeric CPG2 is predicted to undergo active site closure, leading to the putative transition-state complex (on the right), modeled based on the monomeric PepV crystal structure (Supporting Information). For one subunit of the CPG2 dimer, both the zinc-binding domain (red) and the dimerization domain (magenta) are shown. For the second subunit, only the dimerization domain (blue) is shown. Space-filling rendering is applied to the side chains of His229 and Asn263 (blue), Arg288 (magenta), both cocatalytic zinc ions (cyan), the Zn-activated water molecule in the open conformation (red), and the bound transition-state substrate in the closed conformation (colored by atom type with gray carbons). (B) Stereoview of the modeled transition state adduct for CPG2. The tetrahedral intermediate of the 4-(diethylamino)bezoylglutamate substrate, bound at the cocatalytic zinc center of CPG2 in the modeled closed conformation, is shown in sticks representation with carbon, oxygen, and nitrogen atoms colored gray, red, and blue, respectively. The side chains of residues His229, Asn275, Asp286, and Arg288 from the dimerization domains, which correspond to Acy1 residues His206, Asn263, Asp274, and Arg276, respectively, probed experimentally in this study, and the side chain of the putative general base Glu175 (Glu147 in human Acy1), are represented as sticks using the coloring scheme from panel A. The side chains of Zn-chelating residues from the metal-binding domain are also shown with lines. Hydrogen bonds are shown with yellow dashed sticks. Zinc ions are numbered according to Wouters and Husain (*29*). The figure was made with PyMOL (*30*).

hyperbolic behavior, from which a 157-fold increase in K_M and a 57-fold reduction in k_{cat} compared to the wild-type could be estimated, implicating Arg276 in both substrate binding and catalysis.

The D274A mutant showed an almost 5700-fold reduction in catalytic efficiency (Table 2). While the K_M value for D274A remained unchanged, the decrease in k_{cat} for this mutant was the highest observed. Asp274 is the only mutated residue predicted not to directly contact the substrate (cf. Figure 1B). However, this residue appears to be highly important for catalysis.

Enzyme Complementation Assay. We have previously observed that mixing and equilibration of the H206N mutant with mutants of residues in the zinc-binding domain with equally decreased activities, including the putative catalytic base Glu147, led to recoveries of enzymatic activity (*19*). This could be explained by enzyme complementation, that is, the formation of enzyme heterodimers, in which one of

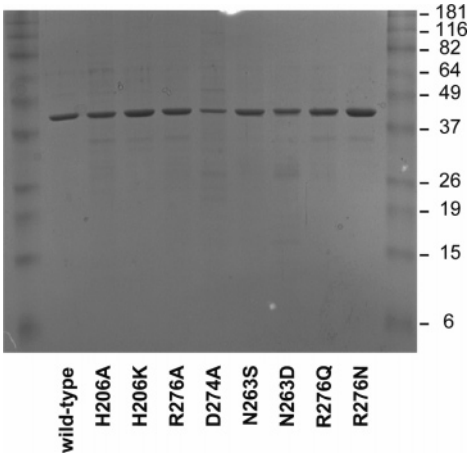

FIGURE 2: Analysis by SDS−PAGE of purified wild-type and mutant Acy1 enzymes after storage at −80 °C for 6−8 months.

Table 2: Kinetic Parameters for the Hydrolysis of *N*α-Acteyl-L-methionine at 20 °C and pH 7.4 of Wild-Type and Mutant Human Acy1 Enzymes

Acy1 variant	k_{cat} (s^{-1})	K_M (mM)	k_{cat}/K_M (fold reduction relative to wild-type)
wild-type[a]	38.3 ± 0.8	0.43 ± 0.03	-
H206N[a]	0.0152 ± 0.0004	2.02 ± 0.15	11837
H206A	0.0859 ± 0.0033	0.54 ± 0.07	560
H206K	0.1486 ± 0.0061	0.58 ± 0.06	348
N263S	0.4577 ± 0.0256	0.78 ± 0.10	152
N263D	not measurable	not measurable	not measurable
R276A	0.6674 ± 0.1636	67.4 ± 18.4	8995
R276N[b]	not measurable	not measurable	16041
R276Q[b]	not measurable	not measurable	60600
D274A	0.0061 ± 0.0003	0.39 ± 0.05	5695

[a] The values for the wild-type and the H206N mutant were taken from ref *19*. [b] The kinetics for R276Q and R276N were linear up to 20 mM.

the two active sites harbored both mutations, while the other remained intact. We concluded that His206 from one dimer subunit is recruited to the active site defined by the zinc-binding domain of the other subunit. This means that catalysis in Acy1 occurs at the dimer interface, and we refer to this as "catalysis *in trans*". Below, we accordingly refer to putative active site residues that reside in the same dimer subunit as acting *in cis*.

As for the H206N mutant (*19*), the activities of our mutants for the dimerization domain residues Asn263, Arg276, and Asp274 were significantly reduced or, in the case of the N263D mutant, not measurable as described above. This prompted us to also experimentally test the relative subunit allocations of these residues in the active site by enzyme complementation. We included the alanine variants of His206 and Glu147 (*19*). Figure 3 summarizes the activities relative to the wild-type enzyme for all possible combinations of the mutants H206A, N263D, D274A, R276A, and E147A in comparison to those for the mutants alone. The results confirm the putative alignment of residues from the different enzyme subunits as outlined above and illustrated by the inserted schematic in Figure 3: only *in trans* but not *in cis* combinations showed higher activities than either of the mutants when assayed alone.

Notably, the apparent inactivation of the N263D mutant was not associated with irreversible unfolding of this protein.

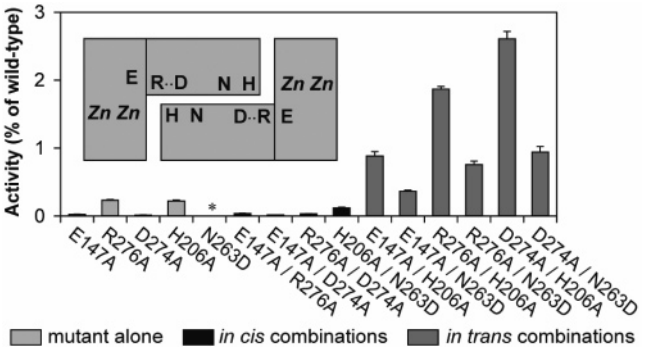

FIGURE 3: Enzyme complementation assay. In the inserted schematic of an Acy1 dimer, *Zn Zn*, E, R, D, N, and H indicate the dinuclear zinc center, Glu147, Arg276, Asp274, Asn263, and His206, respectively. The relative positioning of residues within one subunit of the dimer is referred to as *in cis*, and the relative positioning of residues from opposite dimer subunits as *in trans*. No activity was measurable for the N263D mutant alone (*).

Comparison of the three *in trans* combinations for N263D with those for H206A shows that the recovered activities of the combinations for both mutants increased in the same order (E147A < R276A < D274A). This suggests that both mutants behaved similarly in this assay, even though the values for the combinations involving H206A were more than twice as high as with N263D. The alternative combination of the N263D mutant with R276N (not shown), on the other hand, yielded a 3% recovery, comparable to the D274A/H206A combination.

Overall, the levels of recovery with the dimerization domain mutations introduced here did not exceed 3% of the wild-type activity, compared to 3−24% recoveries in our earlier study, with 16.7% being the calculated maximum theoretical value (*19*). The diminished recoveries for the *in trans* combinations tested here (Figure 3) may indicate that our dimerization domain mutations not only reduce the catalytic activity of the active site in the heterodimer, to which a given residue specifically contributes, but additionally interfere with the formation of the catalytically competent conformation of the second active site. We consider it, however, more likely that in the combinations shown in Figure 3 the mutations alter dimerization itself, so that homo- and heterodimers do not form with equal affinities, and the equilibrium concentrations of the heterodimers were lower than of the two corresponding homodimers, when these are mixed at equimolar ratios. A close to 40% recovery for the alternative *in trans* combination of the H206A and R276N mutants (not included in Figure 3), on the other hand, is most easily interpreted as favored formation of the H206A/R276N heterodimer versus the two mutant homodimers. It appears that the efficiency of heterodimerization is highly dependent on the nature of the combined mutations. Viewed qualitatively, the results shown in Figure 3, nevertheless, confirm the validity of the concept of the complementation assay.

Dimerization Domain Residues in Binding and Catalysis by Acy1. Schneider and co-workers used chemical modification for the investigation of essential residues in porcine Acy1 (*27*, *28*), which shares 88% sequence identity with the human enzyme, including all residues mentioned in this report. Photooxidation and chemical modification of porcine Acy1 provided the first evidence for the importance of histidine residues for the enzymatic activity (*27*). Arguably, His206

(human Acy1 numbering) was one of the residues modified. As already mentioned, the structure of a PepV−inhibitor complex implicated the equivalent residue His269 in transition-state stabilization through oxyanion-binding (*21*). Contrarily, the recent modeling of *N*-carbamylamino acid substrates into the structure of βAS involved the corresponding His262, and also Asn309 and Arg322 (Asn263 and Arg276 in human Acy1, respectively), in the binding of the free carboxyl group of the substrate (*12*). Although such a role cannot be excluded for this histidine in other Acy1/M20 family enzymes, the reductions in k_{cat} for our mutants of His206 in human Acy1 chiefly support a role in catalysis.

The partial degradation, that we observed during the expression of the N263A mutant, is difficult to account for in the absence of a complete Acy1 structure but suggests a function of Asn263 for the proper folding of the protein, which was retained in the N263S and N263D mutants. The kinetic behavior of the N263S mutant resembled those of H206K and H206A, while mutation of Asn263 to aspartic acid had a dramatic effect in that no activity at all could be measured (Table 2). This was likely not as much due to structural perturbations, because the N263D mutant was still functional in enzyme complementation. Instead, these data are consistent with a potential transition-state interaction for Asn263 in Acy1 similar to that seen for the equivalent Asn217 in the PepV−inhibitor complex (*21*): Asn217 binds to the C-terminal carboxylate of the transition-state inhibitor. In the N263D mutant of Acy1, the negative formal charge introduced by the mutation may have compromised the correct assembly of the binary closed complex by repulsion of the negatively charged C-terminal carboxylate of the substrate. It can also be speculated that the proximity of a negatively charged aspartate at position 263 in the mutant to both the zinc center and the transition-state oxyanion (cf. Figure 1B, see Appendix) might have altered the Zn-coordination of the wild-type enzyme and precluded transition-state formation.

Studies of substrates and competitive inhibitors of porcine Acy1 in the laboratory of Schneider further demonstrated that a free carboxyl group is essential for optimal binding to the enzyme (*28*). Chemical modification experiments suggested that a single lysine residue per binding site participated in this interaction (*28*). While the identity of this lysine remains elusive, the fact that mutants of Arg276 could not be fully saturated with substrate during our kinetic analysis (Table 2) identified this residue as a primary substrate-binding residue in the Michaelis complex. Jozic et al. have argued in the case of PepV that domain flexibility is required to allow substrate access (*21*). Accordingly, we hypothesize that complete domain closure and formation of the catalytically competent active site in Acy1 occurs only after an initial binding step reflected by the K_M value. The binding of Arg276 of Acy1 to the substrate likely persists during this conformational change and contributes to transition-state stabilization (reduced k_{cat} for R276A), possibly, through an electrostatic interaction between Arg276 and the free carboxyl group of the ligand as seen in the PepV−inhibitor complex (*21*). Mutation of Asp274, two residues upstream, to alanine also greatly reduced catalytic efficiency. In the crystal structures for CPG2 (*16*) and βAS (*12*), the corresponding residues Asp286 (CPG2) and Asp320 (βAS) do not contribute to the active site directly but serve to anchor Arg288 (cf. Figure 1B, see Appendix) and Arg322, respectively, which are both equivalent to Arg276 of human Acy1. In accordance with our kinetic analysis of the D274A mutant, a similar orientation effect of Asp274 on Arg276 would appear to be dispensable for efficient substrate binding (no change in K_M) but highly important for catalysis (over 6000-fold reduced k_{cat}) by Acy1.

In summary, formation of the catalytically competent active site in the Acy1/M20 family was hypothesized to be associated with a transition from an open to a closed enzyme conformation. Molecular modeling of the closed conformation for the available structure of the CPG2 dimer with a bound transition-state substrate supports the feasibility of such a transition, and the recruitment and appropriate alignment of several residues from both dimerization domains in the active site, which is defined by the dinuclear zinc center of one metal-binding domain. We mutated these residues in human Acy1 followed by enzymatic analyses. We cannot rule out that the measured differences in kinetic parameters for our Acy1 mutants were also affected by structural perturbations as implied by their slightly impaired resistance to proteolysis. Nevertheless, we demonstrate experimentally for the first time for a member of this major group of zinc-dependent amidohydrolases that catalysis occurs at a junction of the zinc-binding domain and the two dimerization domains. Our data suggest important roles in catalysis for Asp274 and Arg276 from the same subunit as the correlated zinc center and for His206 and Asn263 from the opposite subunit. Among these residues, only Arg276 appears to contribute to substrate binding which likely precedes domain closure.

APPENDIX

Substrate-Bound Model of CPG2. In the following description of the modeled transition state adduct for CPG2, residue numbering for human Acy1 is given in parentheses. The transition-state substrate (4-(diethylamino)bezoylglutamate) establishes favorable hydrophobic, hydrogen-binding, and electrostatic contacts with the enzyme. The two oxygen atoms of the tetrahedral diol of the transition state each coordinate one of the two zinc ions (Figure 1B), and these interactions are likely to be preserved in the substrate complexes of Acy1/M20 family enzymes. Moreover, the putative catalytic base Glu175 of CPG2 (Glu147) (*16*) forms two hydrogen bonds with the substrate in the transition state, one with the amide NH of the leaving group and the other with the OH of the tetrahedral adduct (formerly the hydroxylate nucleophile). This modeled geometry, which is not observed in the PepV−inhibitor complex, that lacks the scissile amide bond (*21*), is consistent with a role of Glu175 (Glu147) as the general base in the hydrolysis.

In our CPG2−substrate model (Figure 1B), the invariant His229 residue (His206) from the dimerization domain of one molecule in the dimer contributes to the oxyanion hole together with the Zn1 ion of the other subunit. Arg288 (Arg276) establishes a salt-bridge interaction with the C-terminal carboxylate of the substrate, as seen for the equivalent Arg350 in the PepV complex (*21*). Asp286 (Asp274) serves to anchor and correctly position Arg288 (Arg276), without interacting directly with the substrate. Asn275 (Asn263) is modeled in the proximity of, but not hydrogen-bonded to, the C-terminal carboxylate of the

substrate as seen in the PepV complex (*21*). The Asn275 side chain of the CPG2 model is in the proximity of both the Zn1 ion and the transition-state oxyanion (each at ~5.8 Å from the Asn275 Nδ atom).

SUPPORTING INFORMATION AVAILABLE

Supplemental text outlining the procedures for the modeling of the CPG2-transition state substrate complex based on the published PepV−inhibitor complex. This material is available free of charge via the Internet at http://pubs.acs.org.

REFERENCES

1. Rawlings, N. D., Tolle, D. P., and Barrett, A. J. (2004) MEROPS: the peptidase database, *Nucleic Acids Res. 32*, D160−D164.
2. Schmiedeberg, O. (1881) Über Spaltungen und Synthesen im Thierkörper, *Naunym−Schmiedbergs Archiv. Exp. Pathol. Pharmakol. 14*, 379−392.
3. Jones, W. M., Scaloni, A., Bossa, F., Popowicz, A. M., Schneewind, O., and Manning, J. M. (1991) Genetic relationship between acylpeptide hydrolase and acylase, two hydrolytic enzymes with similar binding but different catalytic specificities, *Proc. Natl. Acad. Sci. U.S.A. 88*, 2194−2198.
4. Xu, F., Byun, T., Deussen, H.-J., and Duke, K. R. (2003) Degradation of N-acylhomoserine lactones, the bacterial quorum-sensing molecules, by acylase, *J. Biotechnol. 101*, 89−96.
5. Nguyen, K. T., and Pei, D. (2005) Purification and characterization of enzymes involved in the degradation of chemotactic *N*-formyl peptides, *Biochemistry 44*, 8514−8522.
6. Breuer, M., Ditrich, K., Habicher, T., Hauer, B., Kesseler, M., Sturmer, R., and Zelinski, T. (2004) Industrial methods for the production of optically active intermediates, *Angew. Chem., Int. Ed. 43*, 788−824.
7. Gröger, H., Trauthwein, H., Buchholz, S., Drauz, K., Sacherer, C., Godfrin, S., and Werner, H. (2004) The first aminoacylase-catalyzed enantioselective synthesis of aromatic beta-amino acids, *Org. Biomol. Chem. 2*, 1977−1978.
8. Taylor, I. N., Brown, R. C., Bycroft, M., King, G., Littlechild, J. A., Lloyd, M. C., Praquin, C., Toogood, H. S., and Taylor, S. J. (2004) Application of thermophilic enzymes in commercial biotransformation processes, *Biochem. Soc. Trans. 32*, 290−292.
9. Klein, J., and Henrich, B. (2004) Peptidase V, in *Handbook of Proteolytic Enzymes* (Barrett, A. J., Rawlings, N. D., and Woessner, J. F., Eds.) 2nd ed., pp 948−949, Elsevier, London.
10. Miller, C. G., and Boder, D. H. (2004) Peptidase T, in *Handbook of Proteolytic Enzymes* (Barrett, A. J., Rawlings, N. D., and Woessner, J. F., Eds.) 2nd ed., pp 946−948, Elsevier, London.
11. Biagini, A., and Puigserver, A. (2001) Sequence analysis of the aminoacylase-1 family. A new proposed signature for metalloexopeptidases, *Comp. Biochem. Physiol.,Part B: Biochem. Mol. Biol. 128*, 469−481.
12. Lundgren, S., Gojkovic, Z., Piskur, J., and Dobritzsch, D. (2003) Yeast β-alanine synthase shares a structural scaffold and origin with dizinc-dependent exopeptidases, *J. Biol. Chem. 278*, 51851−51862.
13. Boyen, A., Charlier, D., Charlier, J., Sakanyan, V., Mett, I., and Glansdorff, N. (1992) Acetylornithine deacetylase, succinyldiaminopimelate desuccinylase and carboxypeptidase G2 are evolutionarily related, *Gene 116*, 1−6.
14. Meinnel, T., Schmitt, E., Mechulam, Y., and Blanquet, S. (1992) Structural and biochemical characterization of the *Escherichia coli* argE gene product, *J. Bacteriol. 174*, 2323−2331.
15. Holz, R. C., Bzymek, K. P., and Swierczek, S. I. (2003) Co-catalytic metallopeptidases as pharmaceutical targets, *Curr. Opin. Chem. Biol. 7*, 197−206.
16. Rowsell, S., Pauptit, R. A., Tucker, A. D., Melton, R. G., Blow, D. M., and Brick, P. (1997) Crystal structure of carboxypeptidase G2, a bacterial enzyme with applications in cancer therapy, *Structure 5*, 337−347.
17. Hakansson, K., and Miller, C. G. (2002) Structure of peptidase T from *Salmonella typhimurium*, *Eur. J. Biochem. 269*, 443−450.
18. Kördel, W., and Schneider, F. (1976) Chemical investigations on pig kidney aminoacylase, *Biochim. Biophys. Acta 445*, 446−457.
19. Lindner, H. A., Lunin, V. V., Alary, A., Hecker, R., Cygler, M., and Menard, R. (2003) Essential roles of zinc ligation and enzyme dimerization for catalysis in the aminoacylase-1/M20 family, *J. Biol. Chem. 278*, 44496−44504.
20. D'Ambrosio, C., Talamo, F., Vitale, R. M., Amodeo, P., Tell, G., Ferrara, L., and Scaloni, A. (2003) Probing the dimeric structure of porcine aminoacylase 1 by mass spectrometric and modeling procedures, *Biochemistry 42*, 4430−4443.
21. Jozic, D., Bourenkow, G., Bartunik, H., Scholze, H., Dive, V., Henrich, B., Huber, R., Bode, W., and Maskos, K. (2002) Crystal structure of the dinuclear zinc aminopeptidase PepV from *Lactobacillus delbrueckii* unravels its preference for dipeptides, *Structure 10*, 1097−1106.
22. Durand, A., Giardina, T., Villard, C., Roussel, A., Puigserver, A., and Perrier, J. (2003) Rat kidney acylase I: further characterisation and mutation studies on the involvement of Glu 147 in the catalytic process, *Biochimie 85*, 953−962.
23. Cornell, W. D., Cieplak, P., Merz, K. M., Ferguson, D. M., Spellmeyer, D. C., Fox, T., Caldwell, J. W., and Kollman, P. A. (1995) A second generation force field for the simulation of proteins, nucleic acids, and organic molecules, *J. Am. Chem. Soc. 117*, 5179−5197.
24. Pittelkow, S., Lindner, H., and Röhm, K. H. (1998) Human and porcine aminoacylase I overproduced in a baculovirus expression vector system: evidence for structural and functional identity with enzymes isolated from kidney, *Protein Expression Purif. 12*, 269−276.
25. Bradford, M. M. (1976) A rapid and sensitive method for the quantitation of microgram quantities of protein utilizing the principle of protein-dye binding, *Anal. Biochem. 72*, 248−254.
26. Palm, G. J., and Röhm, K. H. (1995) Aminoacylase I from porcine kidney: identification and characterization of two major protein domains, *J. Protein Chem. 14*, 233−240.
27. Kördel, W., and Schneider, F. (1977) Identification of essential histidine residues of aminoacylase by photooxidation and by reaction with diethylpyrocarbonate, *Z. Naturforsch., C: J. Biosci. 32*, 337−341.
28. Frey, J., Kördel, W., and Schneider, F. (1977) The reaction of aminoacylase with chloromethylketone analogs of amino acids, *Z. Naturforsch., C: J. Biosci. 32*, 769−776.
29. Wouters, M. A., and Husain, A. (2001) Changes in zinc ligation promote remodeling of the active site in the zinc hydrolase superfamily, *J. Mol. Biol. 314*, 1191−1207.
30. DeLano, W. L. (2002) *The PyMOL Molecular Graphics System*, DeLano Scientific, San Carlos, CA.

BI051180Y